Disentangling Carbon Concentration Changes Along Pathways of North Atlantic Subtropical Mode Water

Daan Reijnders[1], **Dorothee C. E. Bakker**[2], **Erik van Sebille**[1]

[1]Institute for Marine and Atmospheric research Utrecht, Utrecht University, Utrecht, the Netherlands
[2]Centre for Ocean and Atmospheric Sciences, School of Environmental Sciences, University of East Anglia, Norwich, United Kingdom

Key Points:

- Complex interplay of physical and biogeochemical processes influences carbon dynamics in North Atlantic Subtropical Mode Water.
- We split carbon changes along Lagrangian pathways (subduction, persistence, ventilation and export) into mixing and biogeochemical fluxes.
- Subduction from the mixing layer into the mode water chiefly alters modeled dissolved inorganic carbon of Lagrangian parcels, by $+101\,\mu\mathrm{mol\,L^{-1}}$.

Corresponding author: Daan Reijnders, b.j.h.r.reijnders@uu.nl

Abstract

North Atlantic Subtropical Mode Water (NASTMW) serves as a major conduit for dissolved carbon to penetrate into the ocean interior by its wintertime outcropping events. Prior research on NASTMW has concentrated on its physical formation and destruction, as well as Lagrangian pathways and timescales of water into and out of NASTMW. In this study, we examine how dissolved inorganic carbon (DIC) concentrations are modified along Lagrangian pathways of NASTMW on subannual timescales. We introduce Lagrangian parcels into a physical-biogeochemical model and release these parcels annually over two decades. For different pathways into, out of, and within NASTMW, we calculate changes in DIC concentrations along the path (ΔDIC), distinguishing contributions from vertical mixing and biological processes. Subduction leaves the most distinctive fingerprint on DIC concentrations ($+101\,\mu mol\,L^{-1}$ in one year), followed by export out of NASTMW due to densification ($+10\,\mu mol\,L^{-1}$). Most DIC enrichment and depletion regimes span timescales of less than $\sim$30 days, related to algal blooms. However, varying physical and biological processes often oppose one another at short timescales, so the largest net DIC changes occur at timescales of more than 30 days. While the mean ΔDIC for parcels that persist within NASTMW in one year is relatively small at $+6\,\mu mol\,L^{-1}$, this masks underlying complexity: individual parcels undergo interspersed DIC depletion and enrichment, spanning several timescales and magnitudes. Since biological and physical processes both strongly influence DIC concentrations in NASTMW, refining process understanding and models of both domains is important for accurate projections of carbon cycling and sequestration.

Plain Language Summary

Mode waters are relatively thick water masses with homogeneous properties, such as temperature and salinity. The North Atlantic Subtropical Mode Water (NASTMW), found in the Sargasso Sea, is one such water mass. Lying underneath the ocean surface, it comes into contact with the atmosphere during winter, when the ocean surface layer is vigorously mixed due to strong winds, causing the mixed layer to connect with NASTMW. This way, NASTMW can regulate the climate, since it can buffer atmospheric temperature and carbon anomalies during the summer, when there is no surface connection. It is also a conduit for carbon to penetrate beneath the ocean's upper mixed layer. We study NASTMW from the viewpoint of a water parcel that moves with the currents and see how carbon concentrations in the water parcels change along different NASTMW pathways. For each pathway, the carbon concentration changes due to an interplay of physical mixing and biogeochemical processes, for example related to plankton growth and decay. These processes can unfold over different timescales and may counteract or enhance themselves or one another. The largest change in carbon concentration is found when a parcel moves from the upper ocean mixed layer into NASTMW.

1 Introduction

The ocean is both an integral component of the natural carbon cycle, as well as a large sink for anthropogenic carbon emissions. Since 1850, it has taken up 26% of anthropogenic CO_2 from the atmosphere (Friedlingstein et al., 2022). To understand the ocean carbon sink, now and in the future, it is important to understand how the ocean moves carbon from the upper ocean mixed layer through the permanent thermocline, from where it can be further sequestered on timescales of years, decades or centuries. A major conduit through which this occurs is North Atlantic Subtropical Mode Water (NASTMW). It links the ocean interior to the surface on a yearly basis during winter convective events, and is responsible for 20% of the carbon uptake in the 14–50°N latitude band of the North Atlantic (Bates, 2012).

NASTMW, also referred to as Eighteen Degree Water, is a classical example of mode water (Hanawa & Talley, 2001), featuring a thick vertical layer characterized by near-homogeneous properties including temperature, salinity, and oxygen concentration. It is formed during winter, when surface buoyancy loss leads to convection events that deepen the mixed layer in the Sargasso Sea, and through cross-frontal mixing in the southern flanks of the Gulf Stream (Joyce et al., 2013; Davis et al., 2013). Spring stratification caps off NASTMW again, causing it to act as an interannual buffer of wintertime atmospheric anomalies of temperature and carbon (Bates et al., 2002). Gyre circulation and eddy-induced advection allow NASTMW to spread horizontally southwards, causing it to occupy an area much larger than its formation location (Gary et al., 2014). This makes NASTMW also a key regulator of temperature (Sugimoto et al., 2017), organic carbon (Sugimoto et al., 2017), and nutrients (Palter et al., 2005) in the interior of the subtropical gyre. Subsequent destruction of NASTMW occurs primarily through vertical mixing at the top of the layer, but also through diapycnal mixing and along-isopycnal stirring (Billheimer & Talley, 2016).

Current understanding of the role of NASTMW in oceanic carbon uptake is either based on sparse observations (Bates et al., 2002; Bates, 2012; Billheimer et al., 2021) or is inferred from insights into physical mechanisms such as its formation, ventilation and pathways (Davis et al., 2013; Gary et al., 2014; Kwon et al., 2015; Li et al., 2022; Gan et al., 2023). However, a process-based view of how dissolved inorganic carbon (DIC) is transported along pathways from the ocean surface through NASTMW into the ocean interior is lacking.

We investigate how DIC concentrations change along pathways of NASTMW during its formation, persistence, ventilation, and export to better understand which processes alter carbon concentrations along this conduit between the atmosphere and the ocean interior. To do so, we trace virtual parcels of water along pathways into, out of, and within NASTMW using a coupled physical-biogeochemical, eddy-permitting ocean model. Along the pathways of these flow-following Lagrangian parcels, we disentangle the influence of different physical and biogeochemical processes on the local DIC concentration. We then quantify the timescales and magnitudes of DIC depletion and enrichment regimes, defined between local minima and maxima in DIC anomaly time series. Rather than only looking at the bulk change in DIC concentrations along each pathway, we also consider how these changes are distributed between processes and pathways, as well as in time and between a range of timescales. This allows us to better understand the complexity by which different physical and biogeochemical processes affect the DIC content of NASTMW at different moments and timescales.

We focus on timescales of the order of years and less, as most NASTMW parcels have residence times shorter than a year (Gary et al., 2014). We consider parcels that subduct into NASTMW, ventilating parcels, persisting NASTMW parcels, and parcels that are exported due densification. Parcels in this last class are relevant candidates for longer sequestration on timescales of years to decades (the timescale of the gyre interior; Levine et al., 2011).

2 Data and Methods

2.1 Ocean Model Data

To compute Lagrangian parcel trajectories and along-trajectory DIC changes, we use gridded ocean physics and biogeochemistry output data from a global hindcast ocean model at 1/4° degree resolution, comprised of the FREEGLORYS2V4 physics and FREEBIORYS2V4 biogeochemistry products developed by Mercator Ocean International (MOi) for the Copernicus Marine Service. These coupled products have an eddy-permitting resolution, resolving part of the mesoscale eddy regime, which plays a role in mode water formation (Xu et al., 2014; Davis et al., 2013). Ideally, we would use a model set that resolves the full mesoscale or even parts of the submesoscale, as these play important roles in biogeochemical cycles (Lévy et al., 2024). However, an eddy-permitting resolution accommodates the high computational and storage demands from the physical-biogeochemical run (similar to Atkins et al., 2022), and can provide us with a mesoscale process-level understanding. The horizontal resolution of 1/4° is representative of that typically employed in earth system models (Hewitt et al., 2020), and thus also bears relevance to their dynamics. We use versions of both data products on their native Arakawa C-grid, allowing for more precise Lagrangian trajectory computations (Delandmeter & van Sebille, 2019).

The hindcast ocean model does not include data assimilation, such that ocean physics obeys conservation of mass and momentum and biogeochemical budgets are closed. We use a time series between 1995 and 2017, excluding earlier spin-up years. The length of the time series allows us to take into account interannual variability. Since the model is not constrained by observations after its initialization, it may exhibit drift from observed conditions over time. Thus, we use the model in the context of process understanding rather than precise reproduction of observational data.

Ocean physics in FREEGLORYS2V4 are simulated with NEMO version 3.1 (Madec et al., 2013) with the ORCA025 configuration, having a 22 km horizontal resolution at Cape Hatteras and 75 vertical levels (Bernard et al., 2006). Vertical mixing is parameterized using an adaptation of the turbulent closure model by Blanke and Delecluse (1993). Physics are initialized from the EN4 data product (Good et al., 2013) and atmospheric forcings come from 3-hourly ERA-interim reanalysis products from ECMWF (Dee et al., 2011). FREEGLORYS2V4 has an assimilated counterpart, GLORYS2V4, which is extensively described in Garric and Parent (2017). A comparison of the model with observations is found in Supporting Information (SI) Text S1.

Biogeochemistry in FREEBIORYS2V4 is modeled using the intermediate complexity PISCES-v2 model (Aumont et al., 2015). PISCES simulates the carbon cycle, carbonate chemistry, main nutrients (P, N, Fe and Si) and the lower trophic levels of marine ecosystems (phytoplankton, microzooplankton and mesozooplankton) using 24 prognostic variables in total. These tracers are advected and vertically mixed using the hydrodynamics from FREEGLORYS2V4, without horizontal diffusive mixing. Nitrate, phosphate, oxygen and silicate are initialized using data from the World Ocean Atlas (National Oceanographic Data Center (U.S.) Ocean Climate Laboratory et al., 2002) and DIC and alkalinity are initialized with the GLODAP climatology (Key et al., 2004). The model includes atmospheric deposition and riverine input of Fe, Si, N and P, as well as Fe input from sediment. Although a Redfield ratio of C/N/P = 122/16/1 is imposed, cycles of phosphorus and nitrogen are not fully coupled because of nitrogen fixation, denitrification and external sources. Atmospheric pCO_2 is prescribed at the air-sea interface, computed from monthly global CO_2 mole fractions (Lan et al., 2023). A biogeochemical model verification at the global scale is found Perruche et al. (2019).

Near the Bermuda Atlantic Time-series Study (BATS) site (32°10′N, 64°10′) FREEBIORYS2V4 exhibits a trend of increasing salinity-normalized DIC at 10 m depth, by

+0.2 µmol/L/year (see SI Fig. S12). This is roughly a factor 5 smaller than the observed salinity-normalized DIC trend of +1.08±0.05 µmol/kg/year (Bates et al., 2012). Therefore, the input of the model does not accurately represent the observed decadal increase of upper ocean DIC concentrations due to climate change in the Sargasso Sea. We thus only consider the two decades of model data in the context of interannual variability and focus on a process-based understanding of DIC changes along NASTMW pathways. Due to a bias in the model upper ocean salinity trend, the DIC trend at the surface of the Sargasso Sea is mostly between 0 and −1 µmol/L/year. This is further discussed in SI Text S1.

2.2 Definition of NASTMW

NASTMW was first identified by Worthington (1958) as a water mass with a uniform temperature around 18 °C, giving it the moniker Eighteen Degree Water. It is most commonly classified using a temperature range centered around 18 °C, typically as 17–19 °C (Kwon & Riser, 2004; Maze et al., 2009; Forget et al., 2011), with an added stratification constraint that delineates the vertical homogeneity of mode water (Klein & Hogg, 1996; Kwon & Riser, 2004). Alternatively, it is defined through a potential density range with a threshold to delimit low potential vorticity (PV) (Talley & Raymer, 1982; Billheimer & Talley, 2016).

We choose the following constraints for marking Lagrangian parcels as part of NASTMW:

1. Temperature at the location of the parcels is bounded between 17–20.5 °C. The upper bound is higher than the typical 19 °C, since the temperature stratification is slightly stronger in the NASTMW region in the model than in observations, due to model biases (see SI Text S1), similar to the model study of Gary et al. (2014).
2. The local temperature stratification $\partial T/\partial z$ is smaller $0.01\,^{\circ}\mathrm{C\,m^{-1}}$. This is stronger than the constraint of $\partial T/\partial z < 0.006\,^{\circ}\mathrm{C\,m^{-1}}$ stratification of Kwon and Riser (2004), but the same as in Gary et al. (2014).
3. Parcels reside in NASTMW layers of at least 50 m thickness, to exclude thin mixed layers
4. Parcels reside in a contiguous volume of NASTMW of at least $1\times10^{11}\,\mathrm{m^3}$. While this is only on the order of 10^{-4} times the typical winter NASTMW volume, it excludes many small volumes that are shed off from the main NASTMW volume.
5. We only consider NASTMW west of 35°W, to exclude Madeira Mode Water (Siedler et al., 1987).

Constraints 1–3 are similar to those used in Gary et al. (2014) and Kwon et al. (2015), who also investigate Lagrangian pathways of NASTMW in an ocean model, except that they use a slightly lower temperature upper bound of 20 °C. A sensitivity analysis of the NASTMW constraints is found in SI Text S2. With the constraints used, we find an average yearly maximum volume of $9.0\times10^{14}\,\mathrm{m^3}$, close to the NASTMW volume of $9.1\times10^{14}\,\mathrm{m^3}$ found by Joyce (2012) based on observations. This is further discussed in SI Text S2. Although the volume of NASTMW exhibits strong seasonal and interannual variability, we find a strong decrease in NASTMW volume starting in 2010, which agrees with the observed decrease in mode water formation found by Stevens et al. (2020).

Figure 1 shows March and September snapshots of modeled NASTMW thicknesses defined using the above criteria. The imprint of mesoscale eddies on the NASTMW structure can be clearly observed (Fratantoni et al., 2013; Gary et al., 2014). Due to model biases, the modeled NASTMW has its core located farther eastward with respect to observations. This is discussed in SI Text S1. The modeled NASTMW is used here to gain a process-level understanding of how DIC concentrations change along NASTMW pathways.

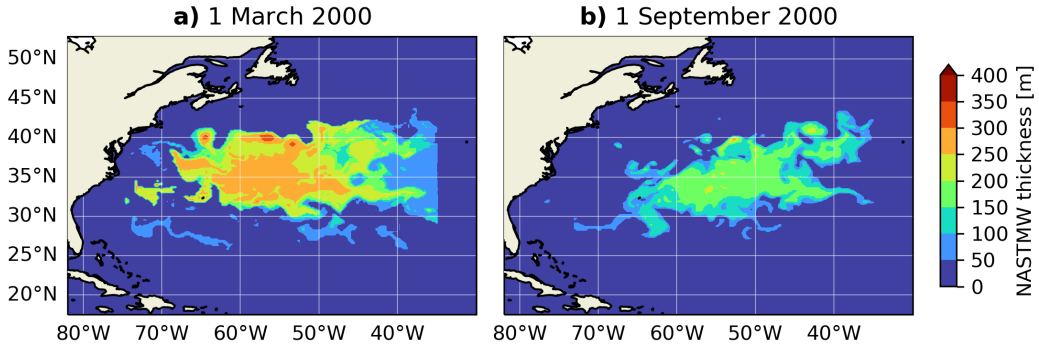

Figure 1. Modeled NASTMW thickness snapshots on (a) 1 March 2000, and (b) 1 September 2000. Note that Madeira Mode Water, east of 35°W, is excluded.

2.3 Initialization and Simulation of Lagrangian Parcels

To compute DIC changes along Lagrangian pathways, we simulate the movement of virtual Lagrangian parcels using the Parcels Lagrangian framework (Delandmeter & van Sebille, 2019) (version 2.4.1). These Lagrangian parcels have no defined size and behave like point particles that are advected using ocean model output velocities, while tracer concentrations are equal to those of the ambient water. Along the Lagrangian pathways, we sample molar concentrations of DIC and its precomputed vertical mixing flux, as well as alkalinity, nitrate, and phosphate and their mixing fluxes (see section 2.5). We also sample temperature, salinity and mixing layer depth, and NASTMW criteria (stratification and contiguity criteria) as these help us distinguish the different NASTMW pathways.

We homogeneously initialize parcels in all parts of NASTMW yearly on 1 September between 1995 and 2015, using to the criteria of section 2.2. Parcels are spaced 30 m apart in the vertical direction, whereas in the zonal and meridional directions we match the horizontal model resolution with a spacing of 0.25°.

Parcels are advected forward and backward in time: forward simulations serve to investigate ventilating parcels, persisting NASTMW parcels, and parcels that are exported due to densification. Backward simulations allow us to investigate which parcels have subducted from the mixed layer since the previous summer. Simulations use time steps of $\Delta t = 90$ minutes. For maximum velocities of the order $\sim 1\,\mathrm{m\,s^{-1}}$ and a nominal grid resolution of 20 km, this is well below the limit of $\Delta t = \Delta x/U = 6$ hours during which a parcel may travel distances at the grid scale. Parcels are simulated for 3 years, although for most of the analysis in this study, we use only the first year of integration data. Locations and biogeochemical concentrations are saved at daily intervals. In total, we simulate a total of 2×861,164 trajectories ($2 \times 20,504 \pm 6,487$ per year, depending on the NASTMW volume), with the factor 2 indicating forward and backward trajectories. The parcel spacing and temporal output are chosen to balance statistical accuracy with the large computational and storage demands from sampling many biogeochemical fields and identifying individual DIC enrichment and depletion regimes (see section 2.6).

Parcel trajectories are computed without adding any stochastic displacements that simulate vertical mixing or subgrid-scale isoneutral dispersion (Reijnders et al., 2022). Instead, the parcels represent the (grid-scale) mean flow. We can then see how subgrid-scale vertical mixing fluxes, which are sampled at parcel locations, influence carbon concentrations at the larger grid-scale.

2.4 NASTMW Pathway Definition

Parcels may enter and exit NASTMW at infinite points in space and time. Here, we delineate four specific pathways into, within, and out of NASTMW. This allows us to focus our assessment on the transformation of DIC concentrations along predefined routes. Figure 2 shows the four (non-exclusive) pathways used in this study. They are defined as follows:

1. *Subduction*: Parcels were in the mixed layer on 1 September in the previous year and end up in NASTMW on the following 1 September. Here, the mixed layer in NEMO is defined as the layer where the temperature is within 0.2 °C of the temperature at 10 m depth. We use the mixed layer rather than the mixing layer (Brainerd & Gregg, 1995) since it is sufficient that in Summer, a parcel has recently been mixed. Relatively few parcels are expected to subduct on timescales of a year. However, using a longer time scale allows parcels to travel larger horizontal distances, thus widening the domain of parcel origin, possibly far beyond the NASTMW formation region. We opt for specifically investigating short subduction time scales of 1 year in order to keep the parcel origin close to the NASTMW region. SI Text S4 discusses results using longer subduction timescales of two and three years.
2. *Persistence*: Parcels persist in NASTMW throughout the year until next September.
3. *Ventilation*: Parcels from September NASTMW at one point reach the mixing layer, defined by the turbocline depth, and are present in NASTMW again next September. The turbocline depth in NEMO is computed by a transition in vertical mixing regimes, where the vertical eddy diffusivity drops below a predefined threshold (Madec et al., 2013). Air-sea heat and carbon fluxes act in the model's upper layer and propagate by vertical mixing throughout the mixing layer. Note that the mixing layer can partially overlap with NASTMW. A portion of persisting NASTMW parcels may thus ventilate as well.
4. *Export*: Parcels leave NASTMW and acquire a potential density that is higher than their last value within NASTMW ($\sigma > \sigma_{\mathrm{NASTMW}}$). We are particularly interested in parcels that persistently maintain their higher densities for a full year, to exclude parcels that only densify temporarily. Since not all parcels will densify immediately when the simulation starts, we here require that parcels have been densified out of NASTMW for at least a continuous year, two years after their initialization. We view these parcels as candidates for sequestration, since they represent previous NASTMW parcels that are transformed and exported to higher density waters. When parcels leave NASTMW, their densities may undergo slightly negative fluctuations. We relax the criterion slightly to allow for this: $\sigma > \sigma_{\mathrm{NASTMW}} - \Delta\sigma$, with $\Delta\sigma = 0.01\,\mathrm{kg\,m^{-3}}$. σ is computed using TEOS-10 (McDougall & Barker, 2011). We discuss variations of $\Delta\sigma$ in the SI Text S4.

Note that we focus on the total, time-integrated, change in DIC along a Lagrangian pathway, indicated by ΔDIC, and on timescale distributions of DIC concentration changes along these pathways. The Lagrangian pathways of NASTMW parcels have already been extensively described from a physical perspective by Gary et al. (2014) and Kwon et al. (2015).

The above four pathways are not exhaustive. For example, between consecutive summers a parcel may temporarily leave NASTMW for a few days without reaching the mixing layer. Such a parcel would not fall into any of the above categories. Other examples are particles that densify without remaining denser than their NASTMW exit density for a year, or parcels that subduct over timescales longer than one year. We deliberately limit ourselves to the four pathways defined above, because their clear definitions help create a process-based understanding of carbon fluctuations throughout the life cycle of NASTMW.

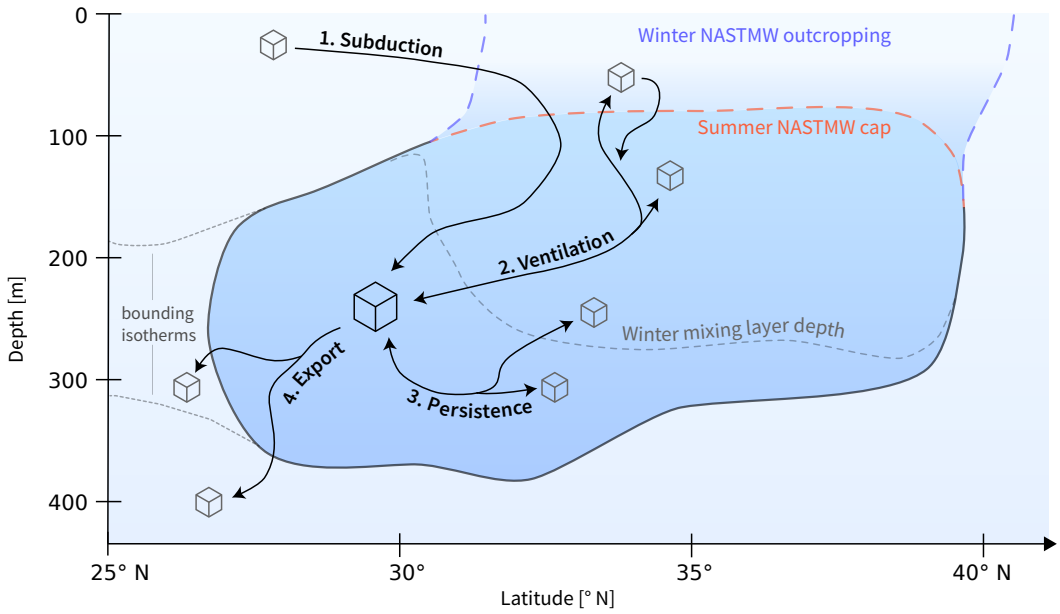

Figure 2. Sketch of the four Lagrangian pathways in and out of NASTMW as covered in this study in latitude-depth space. NASTMW is indicated in dark blue. Actual NASTMW boundaries and outcropping locations also exhibit longitudinal, seasonal and interannual variation.

2.5 Disentangling DIC Fluxes

We distinguish the imprint of physical and biological fluxes on DIC concentrations along Lagrangian trajectories by decomposing the total change in DIC as follows:

$$\frac{\partial[\mathrm{DIC}]}{\partial t} + \mathbf{u}\cdot\nabla[\mathrm{DIC}] = \frac{\partial[\mathrm{DIC}]}{\partial t}_{\text{mixing}} + \frac{\mathrm{D}[\mathrm{DIC}]}{\mathrm{D}t}_{\text{bio}} + \frac{\partial[\mathrm{DIC}]}{\partial t}_{\text{air–sea}} + \frac{\partial[\mathrm{DIC}]}{\partial t}_{\text{residual}}. \quad (1)$$

Here, the left-hand side is the Lagrangian or total derivative of DIC along the pathway, $\frac{\mathrm{D}[\mathrm{DIC}]}{\mathrm{D}t}$. [DIC] in this study is expressed as a molar concentration of DIC, with units $\mu\mathrm{mol\,L^{-1}}$, so that seawater density changes do not affect DIC concentrations in a control volume. The Lagrangian derivative evolves due to vertical mixing into and out of the water parcel, along-trajectory biological sources and sinks, air-sea exchange (only in the surface layer), and residual terms.

The vertical mixing fluxes are computed from the model output vertical diffusivity coefficient k_z and vertical gradients in DIC:

$$\frac{\partial[\mathrm{DIC}]}{\partial t}_{\text{mixing}} = \partial_z(k_z\partial_z[\mathrm{DIC}]). \quad (2)$$

We compute these as daily Eulerian fields and sample them along Lagrangian pathways. Because the model does not include a horizontal mixing parameterization for biogeochemical tracers, we do not include a horizontal mixing term.

Not all PISCES state variables are stored as output in FREEBIORYS2V4: only chlorophyll, nitrate, phosphate, silicate, DIC, total alkalinity, and dissolved oxygen are available. Therefore, we need to approximate the biological sources and sinks from the available variables. We follow Sarmiento and Gruber (2006) and compute the biological flux term as

$$\frac{\mathrm{D[DIC]}}{\mathrm{D}t}_{\mathrm{bio}} = \underbrace{r_{C:P}\frac{\mathrm{D[PO_4{}^{3-}]}}{\mathrm{D}t}_{\mathrm{bio}}}_{\text{soft-tissue}} + \underbrace{\frac{1}{2}\left(\frac{\mathrm{D[TA]}}{\mathrm{D}t}_{\mathrm{bio}} + \frac{\mathrm{D[NO_3{}^{-}]}}{\mathrm{D}t}_{\mathrm{bio}}\right)}_{\text{carbonate}}. \tag{3}$$

Here, the first term on the right-hand side corresponds to soft-tissue production and remineralization. These values are estimated from changes in phosphate concentrations, with $r_{C:P}$ being the Redfield ratio of carbon to phosphorus in PISCES. The second term estimates changes in DIC due to calcite formation and dissolution from changes in total alkalinity, correcting for changes in total alkalinity due to changes in nitrate originating from soft-tissue processes (Brewer et al., 1975). The right-hand side of Equation (3) again consists of Lagrangian derivatives. Note that vertical mixing can also increase or decrease concentrations of phosphate, alkalinity, and nitrate along a Lagrangian trajectory. Rather than a biological effect, this is a physical effect on the DIC concentrations, as already captured in the mixing term in Equation (1). The Lagrangian derivatives of the tracers in Equation (3) are therefore calculated by subtracting their precomputed diffusive mixing fluxes from the total along-trajectory change in tracer concentrations, such that biological effects are isolated. For example:

$$\frac{\mathrm{D[PO_4{}^{3-}]}}{\mathrm{D}t}_{\mathrm{bio}} = \frac{\mathrm{D[PO_4{}^{3-}]}}{\mathrm{D}t} - \partial_z(k_z\partial_z[\mathrm{PO_4{}^{3-}}]), \tag{4}$$

with similar equations for total alkalinity and nitrate.

Explicit air-sea exchange in the ocean model occurs only in the uppermost layer (1 m). Changing DIC concentrations in this uppermost layer will influence the concentrations below by vertical diffusive mixing, as in Equation (2). In our Lagrangian simulations, parcels do not reach the uppermost layer, meaning that they do not experience explicit air-sea exchange. Instead, air-sea exchange only indirectly affects parcel DIC concentrations through strong diffusive mixing in the mixing layer. The air-sea exchange term from Equation (1) in our analysis thus becomes part of the vertical mixing term and is not treated separately. We also cannot differentiate between natural DIC and anthropogenic carbon (C_{ant}; Gruber et al., 1996) since it is not included as a separate tracer in FREEBIORYS2V4.

The residual term captures changes in DIC concentrations that cannot be accounted for by the mixing and biology terms in Equation (1). We compute it by subtracting the biological and mixing fluxes in Equation (1) from the total DIC fluxes along the trajectory. The residual contains the discrepancies between the biological DIC flux computed from Equation (3) and the actual flux in PISCES. It also accounts for unconstrained numerical mixing of DIC and other biogeochemical state variables. Atmospheric and riverine deposition of phosphate and nitrate are neglected when computing their biological changes, thus also leaving an imprint on the residual. We cannot isolate the effects of local freshening or evaporation along Lagrangian parcel trajectories, because these terms cannot be constrained: usually these can be estimated from salinity, but salinity is explicitly horizontally mixed, unlike biogeochemical tracers. Thus, we do not normalize DIC by local salinity in our analysis because horizontal mixing of salinity would cause a drift in the budget over time. In addition, we are explicitly interested in the effect of vertical mixing on DIC concentrations. Evaporation- and precipitation-related freshening directly impact nutrient concentrations only in the model surface layer. Below the first meter, the effect of mixing of fresher and more saline waters on DIC concentrations is part of the mixing term (Equation 2).

To compare the contribution of each flux to $\frac{\mathrm{D[DIC]}}{\mathrm{D}t}$, we compute the sum of the magnitudes of each component. Figure 3a shows the percentage by which each component contributes to this sum of their magnitudes, computed from 1-year trajectories initialized in September 2000 (30-day segments of disentangled time series are found in SI Fig. 35). Our aim is to discern the significance of each flux in determining the ΔDIC across

entire trajectories. To achieve this, we exclude time steps that cumulatively account for less than 5% of the overall flux magnitude sum, thereby focusing on the time steps for which the total fluxes predominantly influence ΔDIC. This method effectively screens out instances with minimal $\frac{\mathrm{D[DIC]}}{\mathrm{D}t}$ values, which are susceptible to disproportionate impacts from numerical inaccuracies, thus distorting the residual's impact. The figure shows that biogeochemical fluxes are the dominant contributor of the total flux at each time step, with soft-tissue processes in turn being the main constituent. As expected, mixing fluxes become increasingly important in the mixing layer. Carbonate and residual fluxes are of similar magnitude.

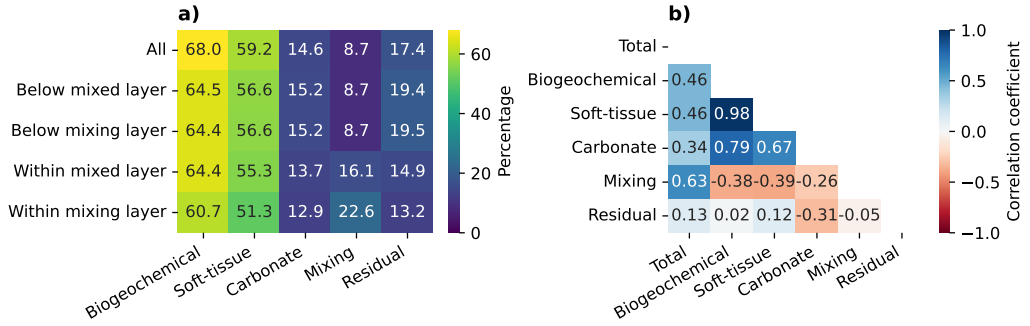

Figure 3. a) Percentage at which each flux contributes to the sum of flux magnitudes, averaged over each time step. Percentages are computed using trajectories initialized in September 2000, selecting only the time steps for which the total flux is responsible for at least 95% of the sum of all total flux magnitudes. We also examine the total biogeochemical flux, composed of the soft-tissue and carbonate fluxes, which may have opposite signs. b) Correlations between each of the fluxes, including the total flux $\frac{\mathrm{D[DIC]}}{\mathrm{D}t}$.

Because the residual flux is composed of multiple unconstrained constituents (see above), we computed correlations between the residual flux and other fluxes. Figure 3b, shows that the residual is only weakly negatively correlated with the carbonate flux and has no appreciable correlation with any other component.

For each water parcel trajectory, we use the disentangled fluxes to reconstruct time series of DIC anomalies with respect to the initial concentration for soft-tissue processes, carbonate processes, vertical mixing, and residual processes.

2.6 Identifying Enrichment and Depletion Regimes and Timescales

One of our aims is to investigate the timescales and strengths at which DIC concentrations are depleted or enriched along NASTMW pathways. We examine both the cumulative ΔDIC along the pathway and intermittent DIC enrichment and depletion *regimes* affecting DIC concentrations.

We have opted for a straightforward approach to define DIC enrichment and depletion regimes. Specifically, these regimes are defined by the intervals in the time series between local minima, which indicate the start of enrichment, and local maxima, which indicate the start of depletion. Thus, the duration of regimes corresponds to the time intervals between these local minima and maxima, whereas the regime's magnitude is the change in DIC concentration during these intervals. In our analyses, we do not truncate regimes that have their start date before the pathway's end date: we analyze trajectories from 1 September till 1 September in the subsequent year (or two years, in case

of export), but if a regime starts before this end date, we still include its entire timescale in our analysis.

To reduce the impact of minor fluctuations occurring over short periods (a few days or less), we apply a centered moving average to the time series. Although this approach smooths the series, it does not completely eliminate short-time variability. Instead, it emphasizes significant changes in DIC concentration, minimizing the influence of brief, minor fluctuations at time scales shorter than the window size. Therefore, the window size partially sets the scale for which regimes are deemed significant. The primary advantage of this methodology lies in its simplicity, offering a clear lens to assess the main dynamics of DIC variations over time. Given our model's nominal resolution of $1/4°$, it does not resolve the submesoscale, which is associated with nutrient transport and biogeochemical structuring at timescales of the order of days (Lévy et al., 2012). Instead, we will apply a window length of 10 days, which is still much shorter than the lifetimes of mesoscale eddies (months) by which nutrients are supplied (McGillicuddy et al., 1998), and instead is of the same order as typical remineralization timescales (Siegel et al., 1999). This allows us to resolve processes on timescales of the order of a week and higher. Additionally, SI Text S5 repeats our analysis without any smoothing, and with smoothing using window sizes of 6 and 20 days. Especially when no smoothing is applied, the bulk of the regime lengths are shorter than 10 days, while their magnitudes are also much smaller. This illustrates the need for smoothing to shed light on processes at longer timescales.

3 Results: DIC Enrichment and Depletion along NASTMW Pathways

For each of the four pathways introduced in section 2.4, we plot the distribution of total ΔDIC per individual parcel that satisfies the pathway's criteria. We also show the relative contribution of biogeochemical, physical and residual processes for different total ΔDIC magnitudes. This will help determine which processes contribute to increasing or decreasing DIC concentrations along each pathway. We also discuss the integrated flux strength of each process per month. Lastly, we examine distributions of enrichment and depletion events spread across timescales and processes.

3.1 The Subduction Pathway

Subduction is investigated by tracing NASTMW parcel pathways backward in time. As can be seen from Figure 4, subduction of parcels into NASTMW has by far the largest impact on DIC concentrations: the mean increase is $\sim 100\,\mu\text{mol}\,\text{L}^{-1}$, though with a large spread for different parcels (Fig. 4a). The dominant contribution comes from vertical mixing, which acts chiefly when the parcel is in the mixing layer. The mixing contribution grows from September until December, after which it decreases to near-zero around May, where it remains steady for the rest of the year (Fig. 4f). This increased mixing coincides with increased downwelling (not shown): upon initialization, parcels experience downwelling at a mean rate of 0.1 m per day in September, increasing steadily to a maximum of approximately 1 m per day in March, after which downwelling velocities reduce again to 0.1 m per day in May. Most parcels exit the mixed layer in April, when the mixing layer shoals again and mixing decreases drastically. In the winter months, when the mixing layer deepens and entrains nutrients, there is a small negative soft-tissue carbon flux from primary productivity (Fig. 4e). Although the spring bloom is visible as a minimum in the mean yearly fifth percentile, subducting NASTMW parcels experience a mean increase in DIC in April, as they move below the mixing layer again. This remineralization flux continues into the following months, as subducting NASTMW is rich in dissolved organic carbon that can be remineralized (Carlson et al., 1994; Krémeur et al., 2009).

We investigate the timescales and magnitudes associated with the enrichment and depletion regimes in Figure 5. Vertical mixing is the dominant contributor across regime timescales (Fig 5a). Only at timescales of 10 days or less, the net ΔDIC is slightly negative. DIC depletion regimes at timescales of 30 days or less primarily occur around March (not shown), during peak primary production. The regime distribution has a long positive tail with around 43% of DIC changes associated with timescales of more than 100 days, mostly associated with vertical mixing. When regime detection is applied specifically to the mixing-related DIC anomaly time series, almost 90% of the ΔDIC is associated with regimes with these long timescales (SI Fig. S37). This shows that vertical mixing steadily increases DIC concentrations as parcels subduct into NASTMW, adjusting to the ambient vertical DIC distribution, with larger DIC concentrations at depth that can supply the parcel with DIC from below (SI Fig. S9).

While the soft-tissue, carbonate and residual fluxes have a relatively minor contribution to the total ΔDIC (Fig. 4c), their contributions are of similar order to the total ΔDIC considered of the other pathways (shown later). The residual and carbonate processes here exhibit the largest contribution (and spread) when parcels are in the mixing layer (SI Fig. 36a & b).

A yearly average of 1.2% of backtracked parcels originate from the mixed layer on the previous September 1st. We also investigated subduction occurring over two and three years. As this allows parcels to subduct over longer timescales, more parcels meet this criterion (3.7% and 5.8% respectively). This is discussed in SI Text S3. In summary, these parcels on average experience a total ΔDIC of similar order ($110\,\mu\text{mol}\,\text{L}^{-1}$ in both cases; see Figs. S13 and S15). While physical mixing is still the dominant contributor in both

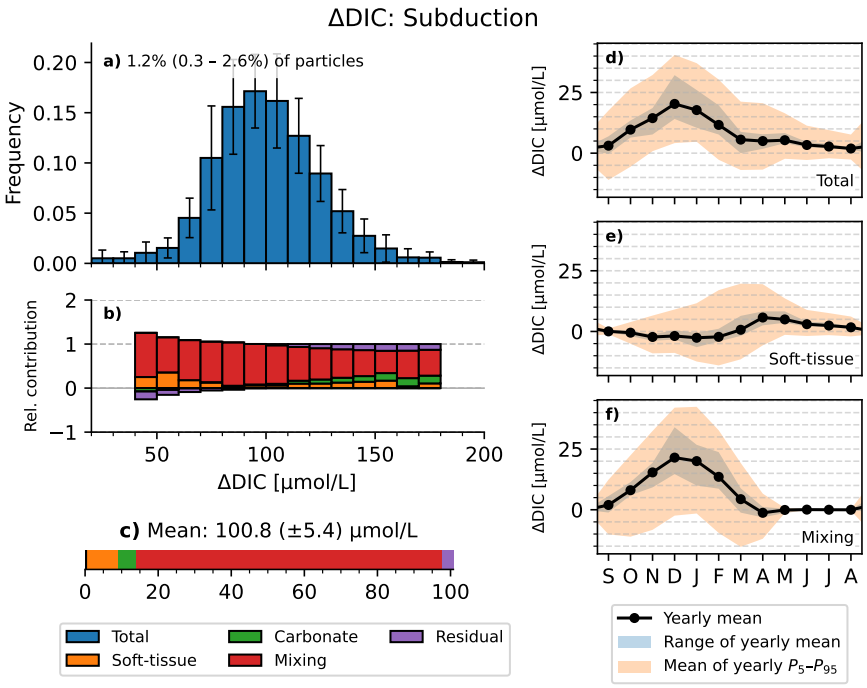

Figure 4. Transformation of DIC concentrations along pathways of parcels that subduct and reach NASTMW. (a) Distribution of total ΔDIC per trajectory for all initialization years 1995-2015. Error bars indicate standard deviation for each bin per year. The average number of trajectories of this pathway is indicated as a percentage of all simulated trajectories per year, with min-max ranges indicated in brackets. (b) Relative contribution of each process to the average ΔDIC, for different ΔDIC strengths. The sum of contributions is always 1, meaning that contributions greater than 1 are balanced by contributions of the opposite sign. The relative contribution is computed only for bins with their edges in the 1st and 99th percentile of ΔDIC. (c) Mean of yearly average ΔDIC of trajectories, with the standard deviation across years in brackets. (d-f) Yearly mean DIC flux, integrated per month, as well as the range of the yearly mean, and the yearly mean of the 5th and 95th percentile, for the total DIC flux (d), soft-tissue fluxes (e), and mixing fluxes (f). Carbonate and residual fluxes are much smaller and are shown in SI Fig. S36 a & b.

cases, soft-tissue processes progressively make up a higher share of the mean total ΔDIC: for subduction over 1 year, these make up 9% of ΔDIC, with this contribution increasing to 20% and 30% when subduction occurs over 2 and 3 years, respectively. These soft-tissue are an important factor in shaping the vertical distribution of DIC (Sarmiento & Gruber, 2006). The longer a parcel takes to subduct, the more time soft-tissue remineralization processes have to directly increase the parcel's DIC, whereas during quick subduction, the parcel will instead adapt its DIC to ambient conditions through mixing.

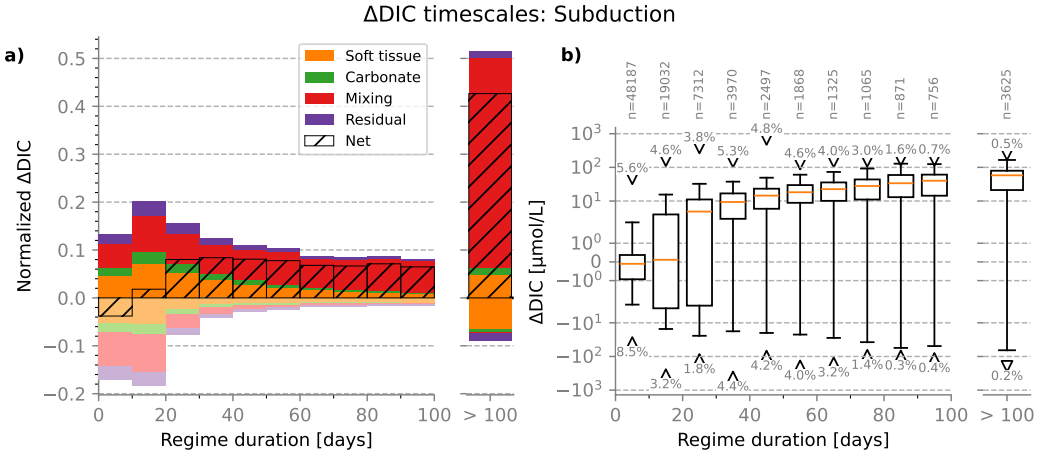

Figure 5. ΔDIC contribution of each timescale for parcels that subduct and reach NASTMW. (a) Relative ΔDIC of regimes of each timescale. This quantity is computed by summing the magnitudes of each positive and negative regime for all trajectories across years and then normalizing by the sum of ΔDIC of each whole trajectory. 'Net' shows the positive minus negative normalized ΔDIC. Because the distribution has a long tail, regimes longer than 100 days are grouped together. (b) Boxplot of ΔDIC magnitudes for each regime for each timescale. Maxima and minima of outliers are indicated by triangles. The number of positive and negative outliers is indicated as a percentage of the total number of regimes, which is indicated above. The boxplot follows the classical definition: whiskers are defined as Q_1-1.5*IQR and Q_3+1.5*IQR (Q_1 and Q3, being the first and third quartile, and IQR=Q_3-Q_1 is the interquartile range). Outliers are defined as regimes with magnitudes that fall outside the whisker ranges.

3.2 The Persistence Pathway

Figure 6, shows the total transformation of DIC concentrations within parcels that persist in NASTMW throughout a full year. On average, this accounts for 25.9% of all parcels, and thus agrees with the model study of Gary et al. (2014), where 74% of NASTMW parcels exit the water mass within a year. Note, however, the large interannual range of parcels that comprise this pathway. The minimum of 2.9% is associated with parcels initialized in September 2013, where the following year of 2014 marked a strong decline in the modeled NASTMW volume toward its minimum in the summer of 2014 (see SI Figure S14). Interannual variability in NASTMW formation and volume is commonly observed (Billheimer & Talley, 2013; Stevens et al., 2020). Generally, we find that the percentage of parcels that persist in NASTMW is correlated with the volume in the next year, with a Pearson-R of 0.88 ($p < 0.001$).

Figure 6b shows that positive contributions are dominated by soft-tissue remineralization, which has a slightly positive monthly mean flux year-round (Fig. 6e). Vertical mixing leaves a distinctly negative imprint on the ΔDIC of persisting NASTMW parcels, meaning that it depletes parcels of carbon. This occurs specifically in winter (Fig. 6f), when the mixing layer deepens, and causes 19% of parcels that persist in NASTMW to have a negative ΔDIC. Because winter mixing is a primary driver of NASTMW formation, some parcels that persist in NASTMW may in fact reside in well-mixed newly formed NASTMW. Vertical mixing can then act to deplete DIC from NASTMW parcels as it is supplied to the euphotic zone. We find that the vertical displacement of a parcel is a predictor for the total ΔDIC (Pearson-R of 0.51, $p < 0.001$): parcels that move deeper, are more likely have increased DIC concentrations. This can be due a smaller likelihood of being temporarily entrained in NASTMW regions that are in contact with the mixing layer.

While the net residual term is smaller than the soft-tissue and mixing terms, the carbonate term is smaller than these residual terms, so we neglect it in our discussion for this pathway. Both the carbonate and residual fluxes show no clear yearly cycle (SI Fig. S36c & d).

From Figure 7 we see that net depletion is associated with timescales of 30 days and less. For timescales between 10 and 30 days, about half of the depletion is attributed to vertical mixing. This is largely associated with the winter convection. The contribution of photosynthesis, a soft-tissue process, has its mode at the 10-20 day timescale, and decays in prominence at larger timescales. Note that the 10-day smoothing of the DIC time series has smoothed out most fluctuations shorter than 10 days. Soft-tissue DIC enrichment, associated with remineralization, has its mode at the 20-30 day timescale, but its tail extends over longer timescales than DIC depletion, with a contribution of almost half the total net ΔDIC at timescales longer than 100 days (see the timescales associated with the soft-tissue DIC anomaly, SI Fig. S38). Figure 7b shows that for timescales less than 20 days, the mode ΔDIC of each individual regime is close zero at timescales less than 20 days and gradually increases to $6.2\,\mu\mathrm{mol\,L^{-1}}$ for timescales longer than 100 days. The net negative ΔDIC at timescales less than 30 days then suggests that strongly negative 'outliers' are responsible for a net decrease at this timescale. For regimes with durations of around a month, we find that these outliers are largely concentrated around March, coinciding with the spring bloom. The spring bloom can thus be linked to strong anomalous DIC depletion for parcels residing in NASTMW.

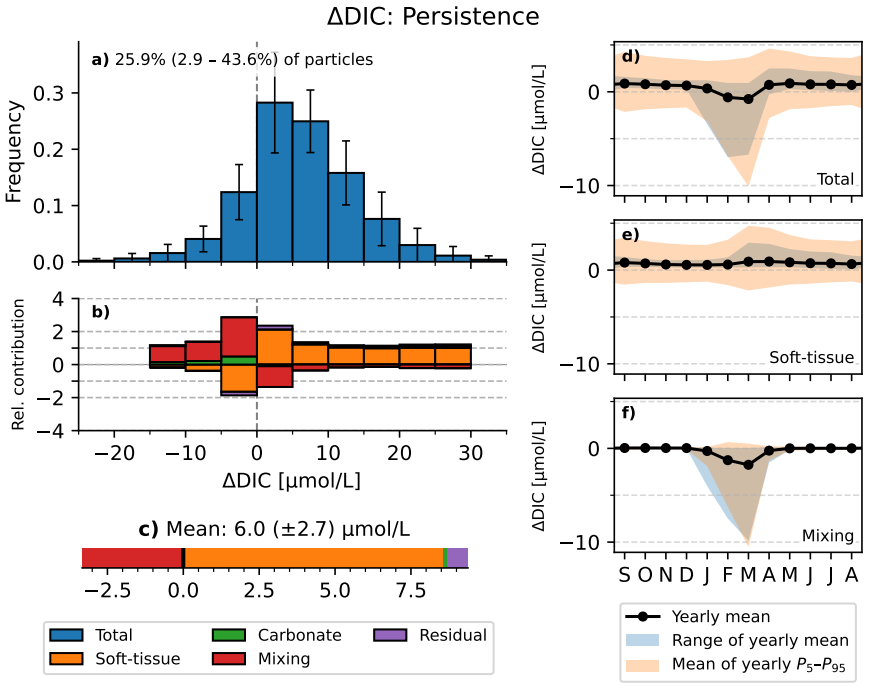

Figure 6. Transformation of DIC concentrations along pathways of parcels that persistently remain in NASTMW. (a) Distribution of total ΔDIC per trajectory, averaged over initialization years 1995-2015. (b) Relative contribution of each process to the average ΔDIC, for different ΔDIC strengths. Note that when the average ΔDIC is negative, positive contributions to ΔDIC (e.g. soft-tissue remineralization) have a negative relative contribution. (c) Mean of yearly average ΔDIC of all trajectories. (d-f) Yearly mean DIC flux, integrated per month, for the total DIC flux (d), soft-tissue fluxes (e), and mixing fluxes (f). Carbonate and residual fluxes are much smaller and are shown in SI Fig. S36c & d.

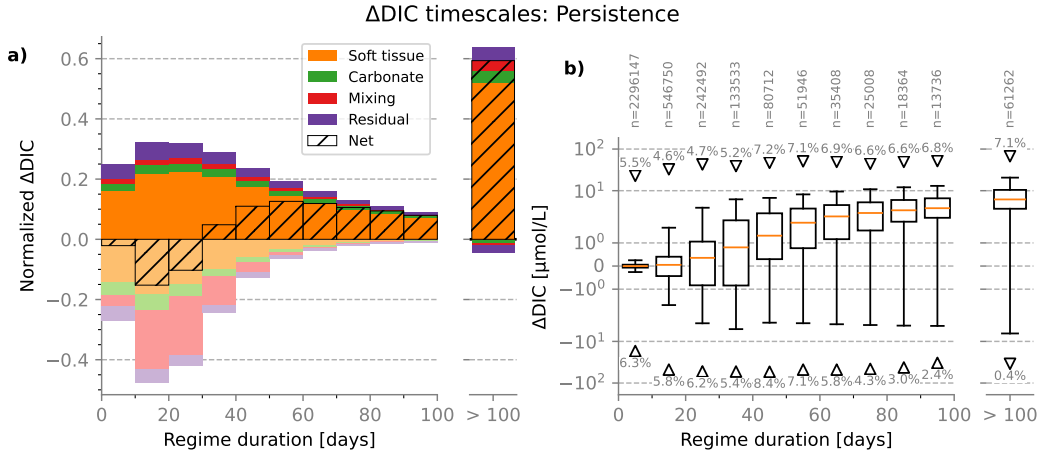

Figure 7. ΔDIC contribution of each timescale for persisting NASTMW parcels. (a) Relative ΔDIC of regimes of each timescale. (b) Boxplot of magnitudes of each regime for each timescale.

3.3 The Ventilation Pathway

On average, parcels that ventilate by temporarily reaching the mixing layer undergo a negligible net ΔDIC (Figure 8). The mean total ΔDIC of $0.7\,\mu mol\,L^{-1}$ is smaller than the interannual standard deviation. However, the ΔDIC distribution for individual trajectories in Fig. 8a is much more spread out. We find that the total ΔDIC along this pathway is correlated with the net downward displacement in the water column with a Pearson-R of 0.60 ($p < 0.001$). Thus, over one yearly ventilation cycle, the net deepening of a particle is a predictor of its increase in DIC.

Figure 8b and c show a strong counteraction of DIC enrichment from soft-tissue remineralization, and a negative contribution for vertical mixing. Figure 8f shows how winter mixing is responsible for the decrease in DIC, as the parcel exchanges its DIC with the mixing layer, supplying nutrients for primary production in the euphotic zone, as well as well as equilibrating with the upper layer in which air-sea fluxes allow for atmospheric gas exchange. Although the mean monthly soft-tissue flux never becomes negative, the mean 5th percentile has a minimum around February and March. This coincides with a modeled maximum in net primary production of phytoplankton, associated with the spring bloom. Only some parcels experience this negative-soft tissue flux directly, as not all parcels can reach the euphotic zone where primary production occurs. Instead, many parcels are linked to spring bloom indirectly, supplying it with nutrients from the deeper parts of the mixing layer. Followed by this, the mean soft-tissue flux has a slight positive maximum in April (Fig. 8e), as the mixing layer shoals and moves above the parcel, allowing organic material to remineralize. The net positive DIC flux remains positive over the following months (Fig. 8d,e). Carbonate processes have a small positive yearly contribution, also peaking in April, after most parcels have left the mixing layer (Fig. S22e). Note that residual processes have no net effect on the ΔDIC for this pathway.

Mixing is the main contributor to the net depletion of DIC at timescales less than 40 days (Fig. 9a). The distribution of DIC enrichment and depletion regimes for ventilating parcels is somewhat similar to that of persisting NASTMW parcels, albeit with a larger contribution from mixing at the short timescales. Fig. 9b shows that the interquartile range and whiskers are symmetric with the median around 0 for timescales less than 20 days, with the median becoming positive at longer timescales. Since the normalized ΔDIC for regimes at timescales less than 30 days is negative, this must be due to strongly depleting outlier regimes, associated with vigorous mixing. In SI Fig. S39, we identify regime timescales and magnitudes based on the DIC anomaly due to mixing processes. Interestingly, we find that about 40% of the net contribution of mixing processes has regime timescales of more than 100 days. When assuming a regime-based view of the total DIC anomaly, the relatively steady DIC depletion due to mixing during wintertime ventilation can be temporarily counteracted by local soft-tissue remineralization, such that mixing is not able to cause the total DIC anomaly to persistently decrease for such long timescales.

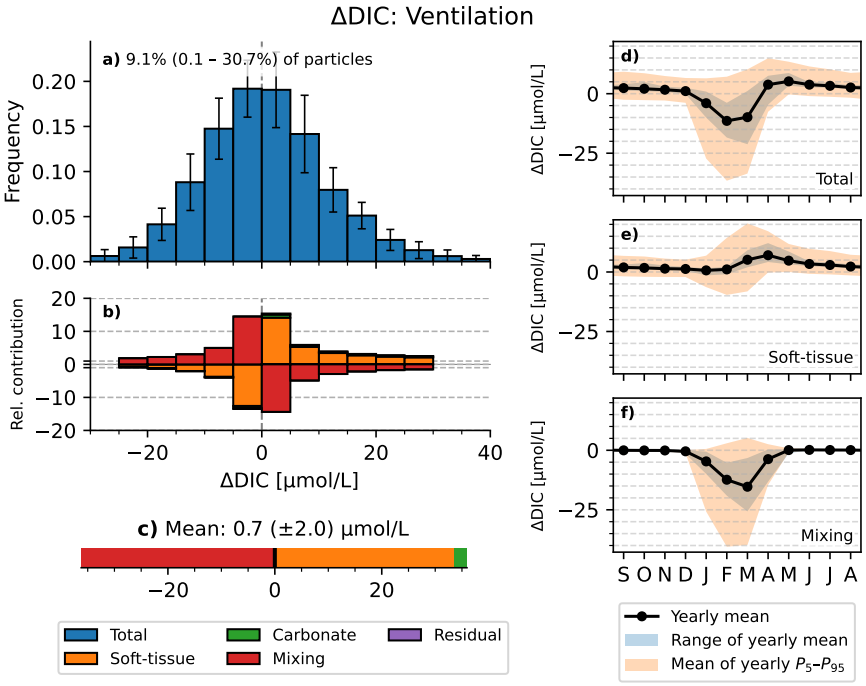

Figure 8. Transformation of DIC concentrations along pathways of ventilating NASTMW parcels. (a) Distribution of total ΔDIC per trajectory, averaged over initialization years 1995-2015. (b) Relative contribution of each process to the average ΔDIC, for different ΔDIC strengths. (c) Mean of yearly average ΔDIC of all trajectories. (d-f) Yearly mean DIC flux, integrated per month, for the total DIC flux (d), soft-tissue fluxes (e), and mixing fluxes (f). Carbonate and residual fluxes are much smaller and are shown in SI Fig. S36e & f.

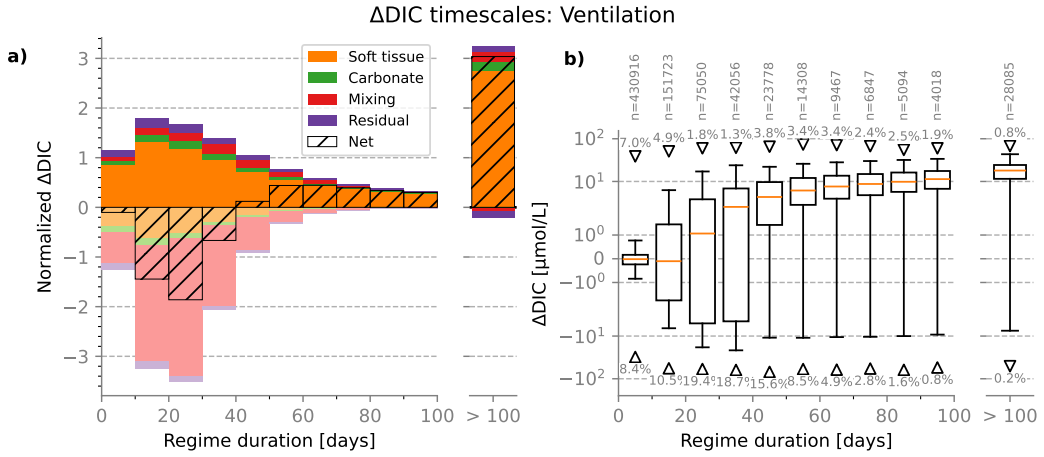

Figure 9. ΔDIC contribution of each timescale for ventilating NASTMW parcels. (a) Relative ΔDIC of regimes of each timescale. (b) Boxplot of magnitudes of each regime for each timescale.

3.4 The Export Pathway

NASTMW parcels that get exported to denser surroundings mostly undergo a net positive ΔDIC (Fig. 10), with a yearly mean of 9.9 µmol L^{-1}. We recall that here, parcels are integrated for a total of two years, during which their potential density remains, for at least the entire second year, higher than their potential density upon exiting NASTMW. 'Exiting NASTMW' here is related to a transformation of the parcel's density or of local stratification, by which NASTMW is destroyed (Kwon et al., 2015).

The distribution of ΔDIC is asymmetric, with a longer tail in the positive direction (Fig. 10a). Soft-tissue processes make up the bulk of the ΔDIC for trajectories in the positive tail (Fig. 10b). Note that for small and negative ΔDIC, the residual becomes more prominent, indicating that the DIC budget becomes less well constrained by our disentanglement method (section 2.5). Mixing fluxes again are concentrated in the winter months of the first year. Due to the way we select exported parcels, some may be temporarily entrained into the mixing layer in the first year of integration. However, outside of the first winter months, the mean DIC fluxes are solely governed by soft-tissue processes. Note that after the first year, these are effectively zero, albeit with the 5th and 95th percentile ranging between values of around ±2 µmol L^{-1} (Fig. 10e), while the residual has a range of ±1 µmol L^{-1} (SI Fig. S36 g & h). Since these ranges are of the same order, while the mean is close to zero, we conclude that after the NASTMW parcels remain exported in the second year, they undergo no clear net DIC depletion or enrichment; the change in ΔDIC occurs before.

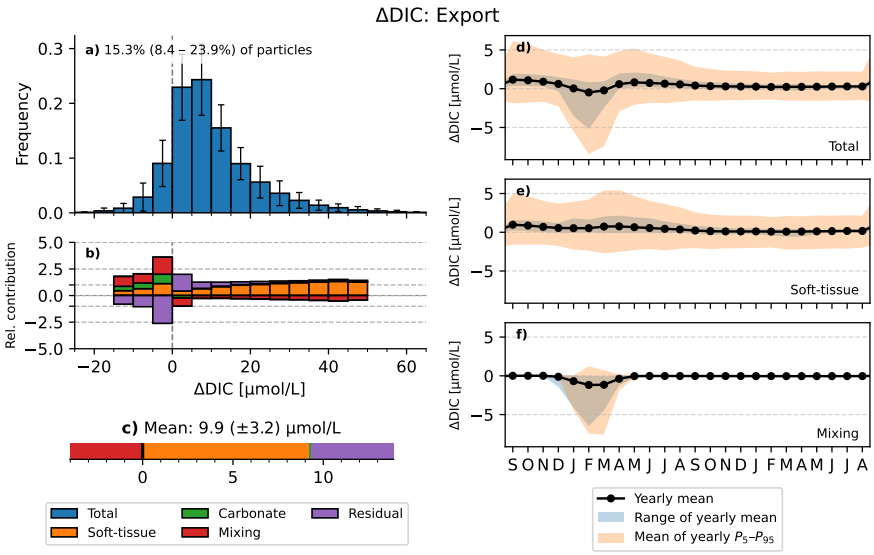

Figure 10. Transformation of DIC concentrations along pathways of exported NASTMW parcels. (a) Distribution of total ΔDIC per trajectory, averaged over initialization years 1995-2015. (b) Relative contribution of each process to the average ΔDIC, for different ΔDIC strengths. (c) Mean of yearly average ΔDIC of all trajectories. (d-f) Yearly mean DIC flux, integrated per month, for the total DIC flux (d), soft-tissue fluxes (e), and mixing fluxes (f). Carbonate and residual fluxes are much smaller and are shown in SI Fig. S36g & h.

Looking at enrichment and depletion regimes and timescales (Figure 11), we see that at short timescales of less than a month, positive and negative ΔDIC regimes nearly balance one another. The net ΔDIC of regimes with longer timescales becomes positive,

dominated by soft-tissue remineralization. Mixing mainly acts to deplete exporting NASTMW parcels of their DIC at timescales of around a month and less, while, photosynthesis and remineralization balance each other out at timescales up to two weeks. At short timescales, the enrichment and depletion magnitudes show a symmetric distribution, also in terms of outliers (Fig. 11b), meaning that at these timescales, there is a balanced counteraction. While the number of parcels that we consider exported depends on the potential

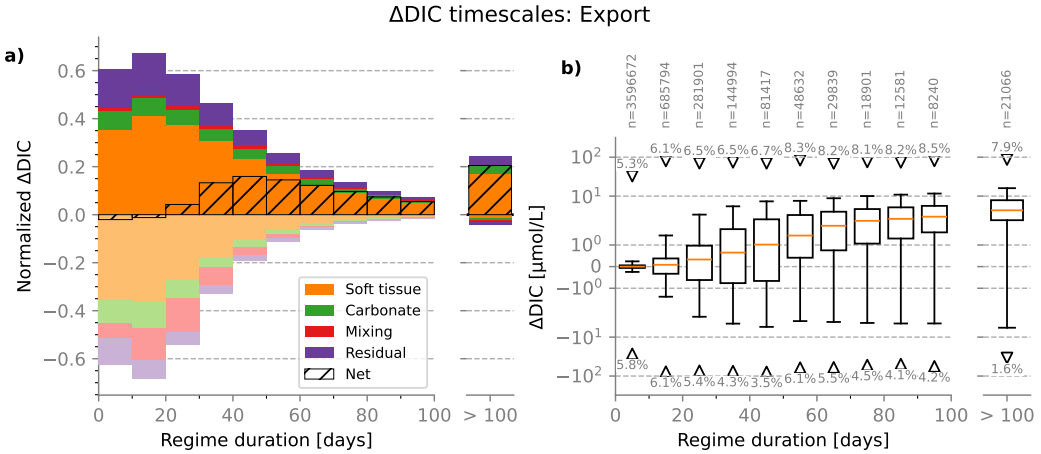

Figure 11. ΔDIC contribution of each timescale for exported NASTMW parcels. (a) Relative ΔDIC of regimes of each timescale. (b) Boxplot of magnitudes of each regime for each timescale.

density threshold, $\Delta\sigma$, these parcels qualitatively exhibit similar total ΔDIC, regime magnitudes and timescales. This is further discussed in SI Text S4.

Pathway	**ΔDIC in model** [μmol L^{-1}]	**Average % of parcels in one simulation**
1. Subduction	100.8	1.2 %†
2. Persistence	6.1	25.9 %
3. Ventilation	0.7	9.1 %
4. Export	9.9 ‡	15.3 %

Table 1. Yearly mean ΔDIC for each pathway in the hindcast model, including mean occurrences. † This percentage increases if we consider long timescales for subduction, with the associated ΔDIC still having a similar magnitude (110 µmol L^{-1} if subduction occurs over 2 or 3 years). ‡ DIC changes mostly occur before the parcel is exported.

4 Summary & Discussion

We adopted a Lagrangian frame of reference to study how dissolved inorganic carbon concentrations are altered along different NASTMW pathways in an eddy-permitting model that reproduces NASTMW for process study purposes. The yearly mean ΔDIC for each pathway, as well as the mean fraction of particles that take each pathway is summarized in Table 1. As mentioned in section 2.4, these pathways are non-exhaustive and non-exclusive, as there is a myriad of paths that parcels may take into and out of NASTMW (e.g. leaving NASTMW temporarily while not ventilating, densifying for less than a year, or subducting over longer timescales than one year).

We found that along different NASTMW pathways, parcels undergo by far the largest DIC enrichment as they subduct from the mixed layer into NASTMW, with an order of magnitude $\sim 100\,\mu\text{mol}\,\text{L}^{-1}$, independent of whether subduction occurs over one, two or three years. The timescale at which subduction occurs determines the partitioning of enrichment and depletion into contributions of physical mixing and biogeochemical process contributions. For rapid subduction from the summer mixing layer to NASTMW in a year, enrichment is almost solely due to vertical mixing, acting to homogenize the parcel's DIC concentration to the surrounding water column, supplying the parcel with nutrients from below. When parcels subduct over more than one year, biogeochemical processes can have a greater direct contribution to net enrichment. Only 1.2% of parcels subducts from the mixed layer into NASTMW between two consecutive Septembers, but this percentage increases as longer subduction time periods are considered.

Parcels that persist in NASTMW during a full year on average undergo a small net enrichment of $\sim 6\,\mu\text{mol}\,\text{L}^{-1}$, with the magnitude of enrichment correlating to net downward displacement of a parcel. Soft-tissue remineralization here counteracts any depletion by vertical mixing that supplies nutrients to the euphotic zone. For the bulk of the parcels, remineralization dominates depletion. This depletion mainly occurs due to vertical mixing in the winter months. Parcels that reside in NASTMW from one summer to the next thus contribute to the nutrient supply in the euphotic zone during March peak primary productivity, after which NASTMW DIC is enriched throughout the year due to remineralization.

Parcels that reside in NASTMW between two consecutive summers may intermediately reach the mixing layer and ventilate. Here, they will undergo net depletion due to vertical mixing, which supplies DIC to the euphotic zone for primary productivity-associated photosynthesis and to the upper model layer for air-sea gas exchange. Some parcels directly supply carbon for photosynthesis. This is followed by enrichment due to remineralization, leading, on average, to almost no net DIC changes. The mean value

of $0.7\,\mu mol\,L^{-1}$ is small and of similar order of magnitude as the upper ocean model DIC trend (SI Fig. S12). However, examining individual parcel trajectories, it becomes clear that NASTMW may locally undergo a much stronger net enrichment or depletion, in correlation with the net downwelling over a ventilation cycle.

Parcels that exit NASTMW and are exported due to density increases undergo a net average increase of about $\sim 10\,\mu mol\,L^{-1}$, primarily due to remineralization. However, this increase largely takes place before the densification occurs. Once exported, DIC fluxes are small and average each other out for at least one year. These exported parcels are important candidates for further sequestration. Whether further transformation of their DIC concentration occurs on larger timescales is beyond the scope of this study, but our results hint at the DIC concentrations of these parcels mainly being set before export, predominantly during their earlier subduction, and to a lesser extent within NASTMW itself.

There is a wide spread in the total ΔDIC for each traversed NASTMW pathway. Moreover, individual parcels undergo DIC enrichment and depletion regimes over a range of timescales and magnitudes, due to a complex interplay of physical mixing and biogeochemical processes. This makes it important to adopt a Lagrangian-based perspective when investigating biogeochemical cycling in a water mass, as bulk Eulerian studies can average out the complexity of enrichment and depletion unfolding over different timescales, as revealed in this study.

We introduced a simple approach of defining enrichment and depletion regimes between local minima and maxima in smoothed Lagrangian DIC anomaly time series. The time window over which the data is smoothed determines the minimum timescales that are revealed by this method, as smoothing can filter out short fluctuations between depletion and enrichment. This is further discussed in SI Text S5. Previous Lagrangian studies that aim to quantify timescales in Lagrangian biogeochemical time series make use of Lagrangian decorrelation timescales (Cetina-Heredia et al., 2018; Brady et al., 2021). However, such metrics assume that Lagrangian biogeochemical time series are stationary, while instead biogeochemical depletion and enrichment is highly dependent on the spatial (vertical and horizontal) and temporal location of the water parcel. Whether a particle experiences depletion or enrichment is highly rooted in its spatial location, for example when a parcel gets entrained (or shed off) from an eddy that experiences high primary productivity. Or a parcel may subduct through the thermocline, such that the importance of vertical mixing, as experienced earlier in the mixing layer, rapidly vanishes. These processes are highly non-linear and non-stationary. This is also why we do not opt for spectral approaches, as most of these are rooted in assumptions of periodicity or stationarity, which does not necessarily hold for our trajectories. Instead, our method reveals regime timescales while staying agnostic about any periodicity.

Model data constraints prevent us from investigating submesoscale processes and variability, as higher resolution model data is not available for large regions over the span of decades. The unresolved submesoscale dynamics have large implications for biogeochemistry, for example by creating fronts that provide short-lived nutrient pulses of just a few days (Lévy et al., 2012; Mahadevan, 2016). We note that when no time series smoothing is applied, timescales of less than 10 days still come to dominate the timescale distribution of enrichment and depletion of DIC. However, this allows brief small-amplitude DIC fluctuations to split up longer, steady changes in DIC, masking such processes (SI Text S5). The findings in this study instead are chiefly related to mesoscale ocean dynamics, with a resolution similar to of that of state-of-the-art earth system models (Hewitt et al., 2020).

Further improvements may also lie in improved disentanglement of biogeochemical fluxes (section 2.5). Due to the limited output of model variables, we cannot constrain the full biogeochemical fluxes as they occur in PISCES. For example, we use the

simplifying assumption that carbonate fluxes can be fully determined from alkalinity, while in reality alkalinity is also affected by nitrification and other processes. Ideally, we would incorporate a complete budget of all biogeochemical tracers that are used internally by PISCES to compute the biogeochemical fluxes.

More generally, we emphasize the balanced and often opposing effects that physical mixing and biogeochemical fluxes play for Lagrangian carbon cycling at different stages of NASTMW pathways. It is thus important to continue improving the model representations of both types of processes, as this will aid in further understanding and quantifying ocean carbon sequestration. This is especially important in the context of rising atmospheric carbon dioxide mole fractions and its impacts on the climate.

Open Research Section

The code to reproduce the results and figures from this paper is available at `https://github.com/OceanParcels/NASTMW_DIC`. Upon acceptance, it will be uploaded to YODA, Utrecht University's persistent data repository, where it will be assigned a DOI. The physical hindcast product FREEGLORYS2V4 was made available by Mercator Ocean International on request, and the biogeochemical hindcast product FREEBIORYS2V4 is available at the Copernicus Marine Service (`https://doi.org/10.48670/moi-00019`). Bottle and DIC data used for model-data comparison in Supporting Information Text S1 are available through the CLIVAR and Carbon Hydrographic Data Office (`https://cchdo.ucsd.edu`). WOA18 data is available at `https://www.ncei.noaa.gov/access/world-ocean-atlas-2018/`. WOA23 data is available at `https://www.ncei.noaa.gov/access/world-ocean-atlas-2023/`. The Parcels Lagrangian framework version 2.4.1 is available at `doi.org/10.5281/ZENODO.7680187`.

Acknowledgments

DR and EvS were supported through funding from the Netherlands Organization for Scientific Research (NWO), Earth and Life Sciences, through project OCENW.KLEIN.085. DCEB was supported by UKRI's (UK Research and Innovation) CHALKY project NE/Y004388/1. We thank Siren Rühs and Jamie Palter for useful discussions and feedback, and Coralie Perruche for help with the FREEBIORYS2V4 product. This study has been conducted using E.U. Copernicus Marine Service Information. Bottle and CTD data along A20 in 2003 and 2012 was supported by the NSF/NOAA funded U.S Global Ocean Carbon and Repeat Hydrography Program.

References

Atkins, J., Andrews, O., & Frenger, I. (2022). Quantifying the contribution of ocean mesoscale eddies to low oxygen extreme events. *Geophysical Research Letters*, *49*(15), e2022GL098672. doi: 10.1029/2022GL098672

Aumont, O., Ethé, C., Tagliabue, A., Bopp, L., & Gehlen, M. (2015). PISCES-v2: An ocean biogeochemical model for carbon and ecosystem studies. *Geoscientific Model Development*, *8*(8), 2465–2513. doi: 10.5194/gmd-8-2465-2015

Bates, N. R. (2012). Multi-decadal uptake of carbon dioxide into subtropical mode water of the North Atlantic Ocean. *Biogeosciences*, *9*(7), 2649–2659. doi: 10.5194/bg-9-2649-2012

Bates, N. R., Best, M. H. P., Neely, K., Garley, R., Dickson, A. G., & Johnson, R. J. (2012). Detecting anthropogenic carbon dioxide uptake and ocean acidification in the North Atlantic Ocean. *Biogeosciences*, *9*(7), 2509–2522. doi: 10.5194/bg-9-2509-2012

Bates, N. R., Pequignet, A. C., Johnson, R. J., & Gruber, N. (2002). A short-term sink for atmospheric CO_2 in subtropical mode water of the North Atlantic Ocean. *Nature*, *420*(6915), 489–493. doi: 10.1038/nature01253

Bernard, B., Madec, G., Penduff, T., Molines, J.-M., Treguier, A.-M., Le Sommer, J., ... De Cuevas, B. (2006). Impact of partial steps and momentum advection schemes in a global ocean circulation model at eddy-permitting resolution. *Ocean Dynamics*, *56*(5-6), 543–567. doi: 10.1007/s10236-006-0082-1

Billheimer, S., & Talley, L. D. (2013). Near cessation of Eighteen Degree Water renewal in the western North Atlantic in the warm winter of 2011-2012. *Journal of Geophysical Research: Oceans*, *118*(12), 6838–6853. doi: 10.1002/2013JC009024

Billheimer, S., & Talley, L. D. (2016). Annual cycle and destruction of eighteen degree water. *Journal of Geophysical Research: Oceans*, *121*(9), 6604–6617. doi: 10.1002/2016JC011799

Billheimer, S., Talley, L. D., & Martz, T. R. (2021). Oxygen seasonality, utiliza-

tion rate, and impacts of vertical mixing in the Eighteen Degree Water Region of the Sargasso Sea as observed by profiling biogeochemical floats. *Global Biogeochemical Cycles*, *35*(3). doi: 10.1029/2020GB006824

Blanke, B., & Delecluse, P. (1993). Variability of the tropical atlantic ocean simulated by a general circulation model with two different mixed-layer physics. *Journal of Physical Oceanography*, *23*(7), 1363–1388. doi: 10.1175/1520-0485(1993)023⟨1363:VOTTAO⟩2.0.CO;2

Brady, R. X., Maltrud, M. E., Wolfram, P. J., Drake, H. F., & Lovenduski, N. S. (2021). The influence of ocean topography on the upwelling of carbon in the Southern Ocean. *Geophysical Research Letters*, *48*(19). doi: 10.1029/2021GL095088

Brainerd, K. E., & Gregg, M. C. (1995). Surface mixed and mixing layer depths. *Deep Sea Research Part I: Oceanographic Research Papers*, *42*(9), 1521–1543. doi: 10.1016/0967-0637(95)00068-H

Brewer, P. G., Wong, G. T., Bacon, M. P., & Spencer, D. W. (1975). An oceanic calcium problem? *Earth and Planetary Science Letters*, *26*(1), 81–87. doi: 10.1016/0012-821X(75)90179-X

Carlson, C. A., Ducklow, H. W., & Michaels, A. F. (1994). Annual flux of dissolved organic carbon from the euphotic zone in the northwestern Sargasso Sea. *Nature*, *371*(6496), 405–408. doi: 10.1038/371405a0

Cetina-Heredia, P., van Sebille, E., Matear, R. J., & Roughan, M. (2018). Nitrate sources, supply, and phytoplankton growth in the Great Australian Bight: An Eulerian-Lagrangian Modeling approach. *Journal of Geophysical Research: Oceans*, *123*(2), 759–772. doi: 10.1002/2017JC013542

Davis, X. J., Straneo, F., Kwon, Y.-O., Kelly, K. A., & Toole, J. M. (2013). Evolution and formation of North Atlantic Eighteen Degree Water in the Sargasso Sea from moored data. *Deep Sea Research Part II: Topical Studies in Oceanography*, *91*, 11–24. doi: 10.1016/j.dsr2.2013.02.024

Dee, D. P., Uppala, S. M., Simmons, A. J., Berrisford, P., Poli, P., Kobayashi, S., ... Vitart, F. (2011). The ERA-Interim reanalysis: configuration and performance of the data assimilation system. *Quarterly Journal of the Royal Meteorological Society*, *137*(656), 553-597. doi: https://doi.org/10.1002/qj.828

Delandmeter, P., & van Sebille, E. (2019). The Parcels v2.0 Lagrangian framework: New field interpolation schemes. *Geoscientific Model Development*, *12*(8), 3571–3584. doi: 10.5194/gmd-12-3571-2019

Forget, G., Maze, G., Buckley, M., & Marshall, J. (2011). Estimated Seasonal Cycle of North Atlantic Eighteen Degree Water Volume. *Journal of Physical Oceanography*, *41*(2), 269–286. doi: 10.1175/2010JPO4257.1

Fratantoni, D. M., Kwon, Y.-O., & Hodges, B. A. (2013). Direct observation of subtropical mode water circulation in the western North Atlantic Ocean. *Deep Sea Research Part II: Topical Studies in Oceanography*, *91*, 35–56. doi: 10.1016/j.dsr2.2013.02.027

Friedlingstein, P., O'Sullivan, M., Jones, M. W., Andrew, R. M., Gregor, L., Hauck, J., ... Zheng, B. (2022). Global Carbon Budget 2022. *Earth System Science Data*, *14*(11), 4811–4900. doi: 10.5194/essd-14-4811-2022

Gan, B., Yu, J., Wu, L., Danabasoglu, G., Small, R. J., Baker, A. H., ... Chen, Z. (2023). North Atlantic subtropical mode water formation controlled by Gulf Stream fronts. *National Science Review*, *10*(9), nwad133. doi: 10.1093/nsr/nwad133

Garric, G., & Parent, L. (2017). *Quality information document for global ocean reanalysis products GLOBAL-REANALYSIS-PHY-001-025* (Tech. Rep. No. CMEMS-GLO-QUID-001-025). Copernicus Marine Service. Retrieved 2023-09-18, from `https://catalogue.marine.copernicus.eu/documents/QUID/CMEMS-GLO-QUID-001-025.pdf`

Gary, S. F., Lozier, M. S., Kwon, Y.-O., & Park, J. J. (2014). The fate of North

Atlantic Subtropical Mode Water in the FLAME model. *Journal of Physical Oceanography*, *44*(5), 1354–1371. doi: 10.1175/JPO-D-13-0202.1

Good, S. A., Martin, M. J., & Rayner, N. A. (2013). EN4: Quality controlled ocean temperature and salinity profiles and monthly objective analyses with uncertainty estimates: THE EN4 DATA SET. *Journal of Geophysical Research: Oceans*, *118*(12), 6704–6716. doi: 10.1002/2013JC009067

Gruber, N., Sarmiento, J. L., & Stocker, T. F. (1996). An improved method for detecting anthropogenic CO_2 in the oceans. *Global Biogeochemical Cycles*, *10*(4), 809–837. doi: 10.1029/96GB01608

Hanawa, K., & Talley, L. D. (2001). Mode Waters. In G. Siedler, J. Church, & W. J. Gould (Eds.), *Ocean circulation and climate: Observing and modelling the global ocean* (pp. 373–386). San Diego: Academic Press. doi: 10.1016/S0074-6142(01)80129-7

Hewitt, H. T., Roberts, M., Mathiot, P., Biastoch, A., Blockley, E., Chassignet, E. P., ... Zhang, Q. (2020). Resolving and Parameterising the Ocean Mesoscale in Earth System Models. *Current Climate Change Reports*, *6*(4), 137–152. doi: 10.1007/s40641-020-00164-w

Joyce, T. M. (2012). New perspectives on Eighteen-Degree Water formation in the North Atlantic. *Journal of Oceanography*, *68*(1), 45–52. doi: 10.1007/s10872-011-0029-0

Joyce, T. M., Thomas, L. N., Dewar, W. K., & Girton, J. B. (2013). Eighteen Degree Water formation within the Gulf Stream during CLIMODE. *Deep Sea Research Part II: Topical Studies in Oceanography*, *91*, 1–10. doi: 10.1016/j.dsr2.2013.02.019

Key, R. M., Kozyr, A., Sabine, C. L., Lee, K., Wanninkhof, R., Bullister, J. L., ... Peng, T.-H. (2004). A global ocean carbon climatology: Results from global data analysis project (GLODAP). *Global Biogeochemical Cycles*, *18*(4). doi: 10.1029/2004GB002247

Klein, B., & Hogg, N. (1996). On the variability of 18 Degree Water formation as observed from moored instruments at 55°W. *Deep Sea Research Part I: Oceanographic Research Papers*, *43*(11-12), 1777–1806. doi: 10.1016/S0967-0637(96)00069-6

Krémeur, A.-S., Lévy, M., Aumont, O., & Reverdin, G. (2009). Impact of the subtropical mode water biogeochemical properties on primary production in the North Atlantic: New insights from an idealized model study. *Journal of Geophysical Research*, *114*(C7), C07019. doi: 10.1029/2008JC005161

Kwon, Y.-O., Park, J.-J., Gary, S. F., & Lozier, M. S. (2015). Year-to-year reoutcropping of Eighteen Degree Water in an eddy-resolving ocean simulation. *Journal of Physical Oceanography*, *45*(4), 1189–1204. doi: 10.1175/JPO-D-14-0122.1

Kwon, Y.-O., & Riser, S. C. (2004). North Atlantic Subtropical Mode Water: A history of ocean-atmosphere interaction 1961–2000. *Geophysical Research Letters*, *31*(19), L19307. doi: 10.1029/2004GL021116

Lan, X., Tans, P., Thoning, K., & NOAA Global Monitoring Laboratory. (2023). *Trends in globally-averaged CO_2 determined from NOAA Global Monitoring Laboratory measurements.* NOAA GML. doi: 10.15138/9N0H-ZH07

Levine, N. M., Doney, S. C., Lima, I., Wanninkhof, R., Bates, N. R., & Feely, R. A. (2011). The impact of the North Atlantic Oscillation on the uptake and accumulation of anthropogenic CO_2 by North Atlantic Ocean mode waters. *Global Biogeochemical Cycles*, *25*, GB3022. doi: 10.1029/2010GB003892

Lévy, M., Couespel, D., Haëck, C., Keerthi, M., Mangolte, I., & Prend, C. J. (2024). The impact of fine-scale currents on biogeochemical cycles in a changing ocean. *Annual Review of Marine Science*, *16*(1). Retrieved from `https://doi.org/10.1146/annurev-marine-020723-020531` (PMID: 37352844) doi: 10.1146/annurev-marine-020723-020531

Lévy, M., Ferrari, R., Franks, P. J. S., Martin, A. P., & Rivière, P. (2012). Bringing physics to life at the submesoscale. *Geophysical Research Letters*, *39*, 13. doi: 10.1029/2012GL052756

Li, K., Maze, G., & Mercier, H. (2022). Ekman transport as the driver of extreme interannual formation rates of Eighteen Degree Water. *Journal of Geophysical Research: Oceans*, *127*(1). doi: 10.1029/2021JC017696

Madec, G., Benshila, R., Bricaud, C., Coward, A., Dobricic, S., Furner, R., & Oddo, P. (2013). NEMO ocean engine (Computer software manual No. 27). Zenodo. doi: 10.5281/zenodo.1464817

Mahadevan, A. (2016). The impact of submesoscale physics on primary productivity of plankton. *Annual Review of Marine Science*, *8*(1), 161–184. doi: 10.1146/annurev-marine-010814-015912

Maze, G., Forget, G., Buckley, M., Marshall, J., & Cerovecki, I. (2009). Using transformation and formation maps to study the role of air–sea heat fluxes in North Atlantic Eighteen Degree Water formation. *Journal of Physical Oceanography*, *39*(8), 1818–1835. doi: 10.1175/2009JPO3985.1

McDougall, T. J., & Barker, P. M. (2011). *Getting started with TEOS-10 and the Gibbs Seawater (GSW) Oceanographic Toolbox*. SCOR/IAPSO WG127.

McGillicuddy, D. J., Robinson, A. R., Siegel, D. A., Jannasch, H. W., Johnson, R., Dickey, T. D., ... Knap, A. H. (1998). Influence of mesoscale eddies on new production in the Sargasso Sea. *Nature*, *394*(6690), 263–266. doi: 10.1038/28367

National Oceanographic Data Center (U.S.) Ocean Climate Laboratory, Conkright, M. E., Locarnini, R. A., Garcia, H. E., O'Brien, T. D., Boyer, T. P., ... Antonov, J. I. (2002). *World Ocean Atlas 2001 : objective analyses, data statistics, and figures: CD-ROM documentation* [Technical Report]. Retrieved from `https://repository.library.noaa.gov/view/noaa/1174`

Palter, J. B., Lozier, M. S., & Barber, R. T. (2005). The effect of advection on the nutrient reservoir in the North Atlantic subtropical gyre. *Nature*, *437*(7059), 687–692. doi: 10.1038/nature03969

Perruche, C., Szczypta, C., Paul, J., & Drévillon, M. (2019). *Quality information document global production centre GLOBAL_REANALYSIS_BIO_001_029* (Tech. Rep. No. CMEMS-GLO-QUID-001-029). Copernicus Marine Service. Retrieved 2023-09-19, from `https://catalogue.marine.copernicus.eu/documents/QUID/CMEMS-GLO-QUID-001-029.pdf`

Reijnders, D., Deleersnijder, E., & Sebille, E. (2022). Simulating lagrangian subgrid-scale dispersion on neutral surfaces in the ocean. *Journal of Advances in Modeling Earth Systems*, *14*(2). doi: 10.1029/2021MS002850

Sarmiento, J. L., & Gruber, N. (2006). *Ocean biogeochemical dynamics*. Princeton: Princeton university press.

Siedler, G., Kuhl, A., & Zenk, W. (1987). The Madeira Mode Water. *Journal of Physical Oceanography*, *17*(10), 1561–1570. doi: 10.1175/1520-0485(1987)017⟨1561:TMMW⟩2.0.CO;2

Siegel, D. A., McGillicuddy, D. J., & Fields, E. A. (1999). Mesoscale eddies, satellite altimetry, and new production in the Sargasso Sea. *Journal of Geophysical Research: Oceans*, *104*(C6), 13359–13379. doi: 10.1029/1999JC900051

Stevens, S. W., Johnson, R. J., Maze, G., & Bates, N. R. (2020). A recent decline in North Atlantic subtropical mode water formation. *Nature Climate Change*, *10*(4), 335–341. doi: 10.1038/s41558-020-0722-3

Sugimoto, S., Hanawa, K., Watanabe, T., Suga, T., & Xie, S.-P. (2017). Enhanced warming of the subtropical mode water in the North Pacific and North Atlantic. *Nature Climate Change*, *7*(9), 656–658. doi: 10.1038/nclimate3371

Talley, L. D., & Raymer, M. E. (1982). Eighteen Degree Water variability. *Journal of Marine Research*, *40*, 757–775.

Worthington, L. (1958). The 18° water in the Sargasso Sea. *Deep Sea Research*

(1953), *5*(2-4), 297–305. doi: 10.1016/0146-6313(58)90026-1

Xu, L., Xie, S.-P., McClean, J. L., Liu, Q., & Sasaki, H. (2014). Mesoscale eddy effects on the subduction of North Pacific mode waters. *Journal of Geophysical Research: Oceans*, *119*(8), 4867–4886. doi: 10.1002/2014JC009861